Chemical Physics 348 (2008) 233–236

Contents lists available at ScienceDirect

Chemical Physics

journal homepage: www.elsevier.com/locate/chemphys

A new interpretation of the scanning tunneling microscope image of graphite

Constantinos D. Zeinalipour-Yazdi [a,b,*], David P. Pullman [b]

[a] Department of Chemistry and Biochemistry, University of California San Diego, San Diego, CA 92093, United States
[b] Department of Chemistry, San Diego State University, San Diego, CA 92182, United States

ARTICLE INFO

Article history:
Received 17 January 2008
Accepted 19 March 2008
Available online 25 March 2008

Keywords:
Scanning tunneling microscopy (STM)
Graphite
HOPG
Tip-artifacts
DFT
Graphene

ABSTRACT

In this work, highly-resolved scanning tunneling microscopy images of graphite basal plane are obtained and theoretical computations are performed to explain the resolution of only half the atoms in STM images of graphite. Our experimental and computational findings indicate that the bright elliptical spots observed in trigonal STM images of graphite may not correspond to carbon positions but to π-states localized above alternate carbon–carbon bonds. This interpretation is based on STM experiments that suggest that the elliptical shape of the bright spots may not be a tip artifact and on simulated STM images of a graphite using orthorhombic unit cells that are in excellent agreement with experimentally obtained images.

1. Introduction

Highly-oriented pyrolytic graphite (HOPG), a synthetic form of graphite, has been used as a standard [1] for STM calibration for over a decade due to the relative ease of imaging in vacuum [2], air [3] and water [4] coupled with the known carbon–carbon distances. A majority of images reported in the literature show only three of the six carbon atoms in a given six-member ring [2,5–8]. They also exhibit a corrugation amplitude that is unexpectedly large for a topographically flat surface. This has been explained by the possibility of imaging a single wave-function [9] and the effect of elastic deformations in response of compressive tip forces [10]. Less frequently, honeycomb-like structures [11,12] have been reported in STM images of graphite which sometimes appear to be in coexistence [13,14] with the more commonly observed trigonal structure.

The resolution of only every other atom in the STM image of graphite has been attributed to the carbon-site structural asymmetry, as suggested by various theoretical calculations [5,7,8,15–17]. This structural asymmetry results in two types of carbon sites, A and B, in which the first lacks and the second possesses a neighbor in the second layer (Fig. 1a). The asymmetry has a direct impact on the electronic structure of A and B carbons. Based on the current interpretation of the STM image of graphite, B sites have an increased electron density near the Fermi level, causing them to appear as bright spots. A sites on the other hand, appear as saddle points, since some of their electron density is shared with the underlying carbon atoms. The minima appear at the H sites, which reside in the center of the hexagons.

Another less commonly discussed feature of the STM image of graphite that requires explanation is the elliptical shape of the bright spots, which reduce the image symmetry to a 2-fold symmetric pattern. This phenomenon has been attributed to an asymmetric tip [2], multiple-tips [18], a slipped surface layer configuration [5,11] that differs from the ideal ABAB stacking sequence, a multiple peak structure of the tunnel-active orbital [19] and to a tilted dz^2-like tip state [20]. It is also conceivable that the elliptical shape could be an artifact due to thermal or mechanical drift in the microscope.

In this paper we obtained high-resolution STM images of graphite basal plane under various scanning conditions and performed theoretical computations to explain the resolution of only half the atoms. We propose that the elliptical spots appearing in most STM images of graphite may not correspond to atoms but to π-states that are localized above carbon–carbon bonds in an alternating fashion reminiscent of Lukesh and Pauling's quinoid structure of graphite [21,22]. While the quinoid structure necessarily entails strong bond length alternation, our proposal does not (Fig. 1b).

2. Experimental and computational details

A vibrationally isolated scanning tunneling microscope by Carl Zeiss Jena GmbH, was used in this study. Modifications to the STM base reduced significantly mechanical/thermal drifts and

* Corresponding author. Present address: University of Cyprus, Department of Chemistry, 75 Kallipoleos Street, P.O. Box 20537, 1678 Nicosia, Cyprus. Tel.: +357 22 892815; fax: +357 22 892801.
E-mail address: zeinalip@ucy.ac.cy (C.D. Zeinalipour-Yazdi).

0301-0104/$ - see front matter © 2008 Elsevier B.V. All rights reserved.
doi:10.1016/j.chemphys.2008.03.019

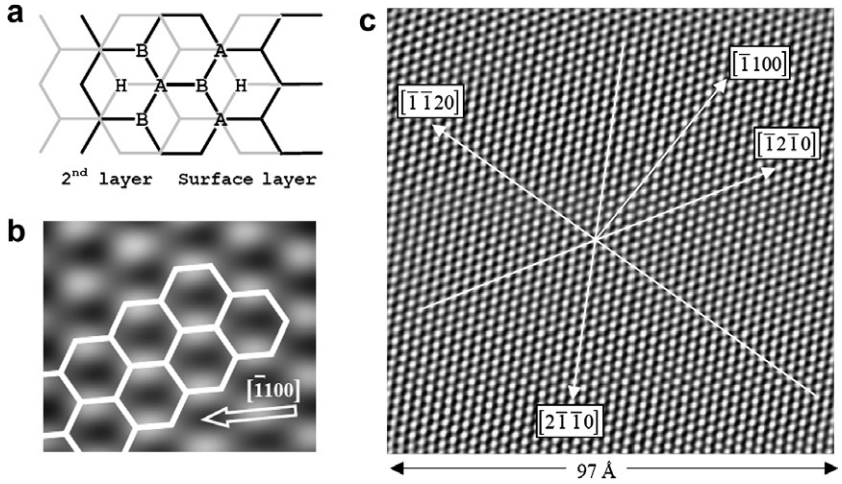

Fig. 1. (a) Schematic representation of the atom assignment in hexagonal graphite. Black line and gray line represent surface and second layer, respectively, (b) graphite lattice superimposed on a constant–current STM image of graphite (I_t = 1.1 nA and sample V_{bias} = −0.1 V) showing atom assignment based on our interpretation. Note that the honeycomb lattice is shifted by half a C–C bond (71 pm) along the direction indicated by the arrow if compared to the atom assignment proposed by references [2,5,7,8]. (c) Another constant–current STM image of graphite (I_t = 1.2 nA and sample V_{bias} = −0.1 V), where [$\bar{1}$2$\bar{1}$0], [$\bar{1}\bar{1}$20] and [2$\bar{1}\bar{1}$0] are the lattice vectors of hexagonal graphite whereas [$\bar{1}$100] indicates the direction spot elongation. Images were Fast Fourier transformed to eliminate high frequency components due to electronic noise.

perturbations by vibrational noise. A sample of highly-oriented pyrolytic graphite (HOPG, ZYA-grade) of low mosaic spread (<0.4° ± 0.1°) was attached to the sample holder which was mounted to 3 piezoelectric crystal tubes ($BaTiO_3$), for movement in the XY directions. An electro-chemically etched (KOH, DC, 3 V) tungsten wire (0.25 × 10.0 mm) was mounted on the central piezoelectric crystal responsible for the movement in the z direction.

All computed STM images were obtained by a home-made program written in Python [23] using the wave-functions derived from the planewave density functional formalism implemented in the NWChem [24] code. The surface of graphite is modeled with a four layer slab separated by a 10 Å vacuum gap in the direction perpendicular to the basal plane (Fig. 2). Unit cells of hexagonal (2 × 2) and orthorhombic (1 × 1) symmetries were studied. The valence one-electron wave-functions were expanded using a plane wave basis, and periodic boundary conditions were invoked. For the hexagonal unit cell a 136 × 34 × 34 k-point mesh, which corresponds to a kinetic energy cutoff of 128 Ry and a planewave expansion of 34,436 sinusoidal waves was used. This ensures energy convergence to less than 10^{-3} eV. The exchange and correlation effects are considered within the generalized gradient approximation (GGA) using the PBE96 [25] exchange-correlation (XC) functional. The electronic core was described by the Hamann [26] norm-conserving pseudopotentials in which the core radii r_{cl} for the various orbitals (l = s,p,d) were set [27] to, 0.80 α_0, 0.85 α_0 and 0.85 α_0, respectively (α_0 = bohr radius). For the hexagonal unit cell slab the lattice parameters were a = 20.000 Å, $b = c$ = 4.912 Å, α = 120°, and $\beta = \gamma$ = 90°, and for the orthorhombic unit cell slab they are a = 2.456 Å, b = 4.254Å c = 20.000 Å, and $\alpha = \beta = \gamma$ = 90°. All carbon–carbon bonds were set to 1.418 Å and the interlayer separation to 3.354 Å based on the crystal structure [28–30].

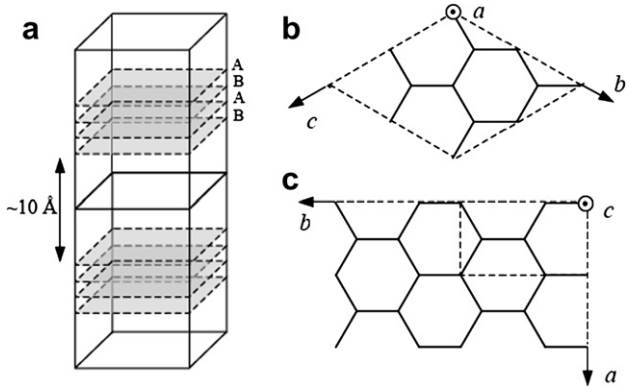

Fig. 2. Schematics of the four layer slab unit cell used in simulations. (a) Schematic representation of two adjacent unit cells showing the arrangement of the four graphite layer, (b) and (c) show the oblique hexagonal (2 × 2) and orthorhombic (1 × 1) surface unit cell of graphite, respectively. The axis not shown points into the plane of the paper.

To obtain the simulated STM images we employ the Tersoff–Hamann [31] treatment for the tunneling current. The surface is treated *exactly*, while the wave-function at the tip is assumed to have spherical symmetry (s-orbital). Since we were interested only in the shape and periodicity of the features in the STM image rather than the absolute tunneling current, we used the local electron density near the Fermi level in our simulations. This density is given by

$$\rho(r, E_F) \equiv \sum_v |\Psi_v(\vec{r}_0)|^2 \cdot \delta(E_v - E_F),$$

where $\Psi_v(\vec{r}_0)$ is the unperturbed surface eigenstate at the tip center of curvature, E_F is the Fermi level energy and E_v is the eigenvalue of $\Psi_v(\vec{r}_0)$. A lateral resolution of 0.05 Å was used in all electron density maps to obtain smoothly varying landscapes.

3. Results and discussion

In this work the following approach was employed. First we establish the symmetry observed in STM images of graphite by examination of high-resolution STM images of HOPG. Subsequently, we exclude the possibility of experimental artifacts (tip convolution, mechanical/thermal drift) that could cause lower symmetry in STM images of graphite. Finally, we simulate STM images of hexagonal graphite using density functional theory and compare these to experimental images.

Although many theoretical calculations [2,5–8] yield a trigonal symmetry (3-fold) in the simulated STM image of graphite, most experimental STM images obtained in our lab and reported in the scientific literature [2,3,15,18,20] lack such high symmetry. This can be seen in Fig. 1c which is a constant–current STM image of HOPG obtained in air. The STM spots are elliptical, having their

long axis along the $[\bar{1}100]$ lattice direction. The result is a 2-fold symmetric pattern where every other carbon atom is missing. Similar images were obtained by us with Pt/Ir tunneling tips at various tunneling conditions. Honeycomb-like patterns were also observed, although their resolution and clarity was significantly lower than the STM patterns presented here.

It is well known that the tunneling current decays exponentially with tip-to-surface separation. Thus, small asymmetries in the electron density distribution at the tip apex near the Fermi level are expected to significantly affect the tunneling current in the STM image. This phenomenon can add artificial features, such as elliptical instead of circular spots, to the STM image that have previously been ascribed to an asymmetric tip [2] or to the orbital structure at the tip apex [19,20]. Additionally, a double tip [18] can have a similar effect since such a tunneling tip may generate images that are the superposition of two images separated by the distance of two atoms at the tip apex.

In Fig. 3a, we present an experimental constant current STM image of HOPG at a tunneling current of 1.1 nA and a sample bias voltage of −0.1 V relative to the tip. A second image of the same area (Fig. 3b) was imaged under identical tunneling conditions after changing the scanning direction (direction that the tip scans with respect to the surface) by 13° counterclockwise. The presence of the graphite step on the left side of the image ensures that we sampled the same area after changing the scanning direction. It is evident that the direction of the spot's long axis changes according to the scanning direction. This suggests that the elliptical shape in these STM images may not be a tip artifact [2,18–20] or an effect of mechanical/thermal drift, since these artifacts would keep the direction of the long axis $[\bar{1}100]$, unaltered.

Simulated STM images of hexagonal graphite were also obtained for a tip-to-surface separation of 2.5 Å using the Tersoff–Hamann model. [31] In principle, only states with energies in the range E_F–eV_{bias} to E_F, and which are in close physical proximity to the tunneling tip will contribute significantly to the tunneling current. In order to test the effect of the bias voltage, low (−0.1 V) and high (−0.7 V) bias voltage simulations are performed. A low bias voltage in these simulations essentially means that a few of the highest occupied crystal orbitals at the Fermi level are sampled.

Isosurfaces of the highest occupied crystal orbitals (HOCOs) close to the Fermi level (Fig. 4a and b) reveal that the shape and location of the orbitals is identical to that of the classical π-orbital seen in ethylene. Crystal orbitals lower in energy (Fig. 4c) occupy the space between the previously mentioned crystal orbitals and form a diffuse electron distribution around each 6-membered carbon ring.

A comparison between experimental and simulated STM images of graphite obtained at low and high bias voltage is given in Fig. 5. Both the hexagonal supercell (2 × 2) and the orthorhombic unit cell (1 × 1) gave the characteristic 2-fold STM pattern observed experimentally, at low bias voltage. Additionally we were able to obtain a honeycomb-like pattern by changing the sample bias voltage from −0.1 to −0.7 V. This was done by summing over a larger number of occupied orbitals at the Fermi level. The transition between the two patterns by changing the tunneling conditions is consistent with the simultaneous [11,12] or even coexisting [13,14] imaging of both patterns reported by previous investigators. In the 2-fold symmetric patterns the bright spots are elliptical rather than circular, and there is a complete absence of the A-type carbon atom. Additionally, our STM simulations are consistent with experimental findings that indicate that the 2nd layer may not be the reason for the resolution of every other carbon atom in the STM image of graphite. Land et al. [32] found that a graphitic monolayer on Pt (1 1 1) has an identical STM image to that of bulk graphite. Our findings are in agreement with this phenomenon since simulations of a single layer of graphite (graphene) modeled by a 5 × 5 orthorhombic supercell yields a 2-fold symmetric pattern at low bias voltage (−0.1 V). This pattern is in good agreement with the typical experimental STM image of graphite shown in Fig. 1c in which bright spots appear elliptical instead of circular and the distance between them is 2.456 Å.

The electronic structure distribution near the Fermi level observed in our STM simulations is in partial agreement with the existence of quinoid structure for graphite [22]. While the quinoid structure necessarily entails strong bond length alternation in our model all carbon–carbon bond lengths were kept equal in accordance with a hexagonal or orthohexagonal (1 × 1 orthorhombic) unit cell, as assigned by X-ray [28] and neutron [30] diffraction

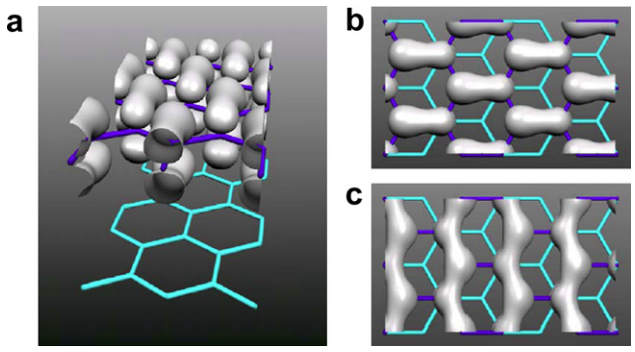

Fig. 4. Isosurfaces of crystal orbitals at the Fermi level of the orthorhombic unit cell. (a and b) Superposition of degenerate pair highest occupied crystal orbitals (HOCO + HOCO − 1) in perspective view and view along [0 0 0 1], respectively. Only wavefunctions in the surface layers are shown for better clarity. (c) HOCO − 5 crystal orbital appears complementary to the HOCO + HOCO − 1 indicating a uniform electron distribution around the carbon rings when electron density is summed over a larger energy window.

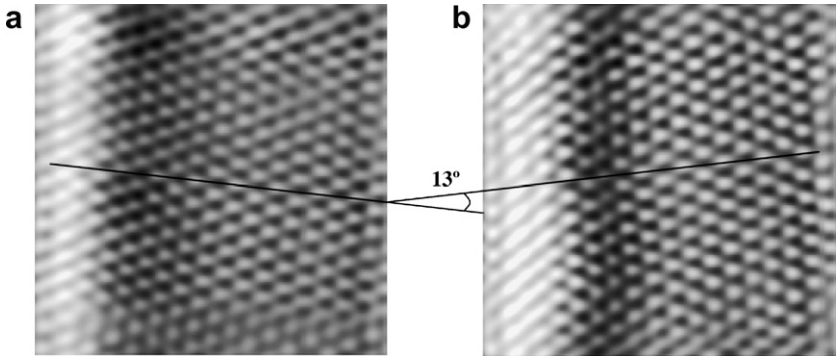

Fig. 3. Effect of scanning direction on STM image of HOPG taken in air (FFT). (a) I_t = 1.1 nA, V_{bias} = −0.1 V. Image dimensions 38 × 38 Å and (b) same tunneling conditions as previous but counterclockwise rotation by 13°.

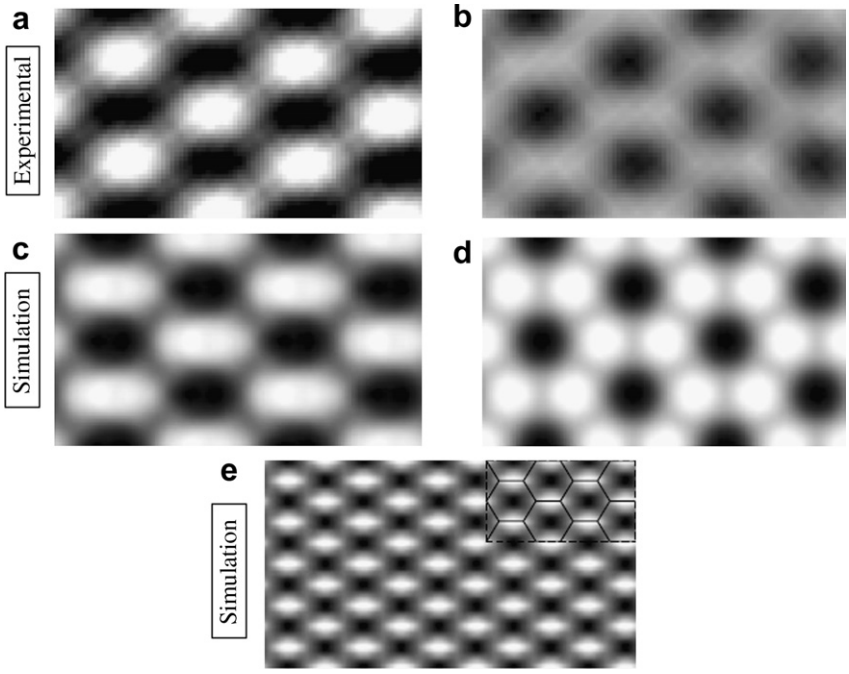

Fig. 5. Comparison between experimental and simulated STM images of graphite. (a and b) Experimental STM images of graphite and (c and d) simulated STM images of the orthorhombic graphite slab obtained at a sample bias voltage of −0.1 V and −0.7, respectively. (e) Simulated STM image of a single graphite layer (graphene) at $V_{bias} = -0.1$ V using a 5×5 orthorhombic supercell.

techniques. Nevertheless, in the simulated STM images of graphite a distinct 2-fold symmetry was observed, thus we propose that the origin of the 2-fold symmetry observed in STM images of graphite may be a result of quinoid-like electronic structure distribution at the Fermi level. This electronic distribution is argued to be more stable [22] due to closer stacking and enhanced London interactions between the graphene layers. It should be further noted that the presence of a small degree of bond length alternation ($\delta < 0.003$ Å) is not to be excluded on the basis of the resolution limit of crystallographic techniques.

4. Conclusions

We have presented evidence that the reduced symmetry (elliptical bright spots) observed in most STM images of graphite may not be a tip artifact, but inherent to the surface electronic structure of graphite. Our STM simulations using the Tersoff–Hamann model are in good agreement with the experimental images we obtained. They exhibit the experimentally observed 2-fold symmetry and have relatively large corrugation amplitude. The bright spots appear elliptical instead of circular and the distance between them is 2.456 Å, as observed experimentally. We also show that a honeycomb-like pattern can be obtained using a higher bias voltage. Thus, we conclude that the protrusion in low bias voltage STM images of graphite may correspond to π-orbitals localized above carbon–carbon bonds. This suggests that the origin of contrast in STM images of graphite could be native to the electronic structure of even a single sheet of graphite, and that the effect introduced by the second layer and various tip-artifacts may not be necessary to explain the image.

Acknowledgement

Professor Annabella Selloni and Dr. Eriketi Loizidou are gratefully acknowledged for useful discussions. We also thank PURE Biosciences of El Cajon, CA for partial funding support of the computer resources.

References

[1] V.Y. Yurov, A.N. Klimov, Rev. Sci. Instrum. 65 (1993) 1551.
[2] G. Binnig, H. Fuchs, C. Gerber, H. Rohrer, E. Stoll, E. Tosatti, Europhys. Lett. 1 (1986) 31.
[3] S.I. Park, C.F. Quate, Appl. Phys. Lett. 48 (1986) 112.
[4] J. Schneir, R. Sonnenfeld, P.K. Hansma, J. Tersoff, Phys. Rev. B 34 (1986) 4979.
[5] I.P. Batra, N. Garcia, H. Rohrer, H. Salemink, E. Stoll, S. Ciraci, Surf. Sci. 181 (1987) 126.
[6] C.T. Lee, W.T. Yang, R.G. Parr, Phys. Rev. B 37 (1988) 785.
[7] A. Selloni, P. Carnevali, E. Tosatti, C.D. Chen, Phys. Rev. B 31 (1985) 2602.
[8] D. Tomanek, S.G. Louie, Phys. Rev. B 37 (1988) 8327.
[9] J. Tersoff, Phys. Rev. Lett. 57 (1986) 440.
[10] J.M. Soler, A.M. Baro, N. Garcia, H. Rohrer, Phys. Rev. Lett. 57 (1986) 444.
[11] P.J. Ouseph, T. Poothackanal, G. Mathew, Phys. Lett. A 205 (1995) 65.
[12] J.I. Paredes, A. Martinez-Alonso, J.M.D. Tascon, Carbon 39 (2001) 476.
[13] P. Moriarty, G. Hughes, Appl. Phys. Lett. 60 (1992) 2338.
[14] Y. Wang, Y. Ye, K. Wu, Surf. Sci. 600 (2006) 729.
[15] D. Tomanek, S.G. Louie, H.J. Mamin, D.W. Abraham, R.E. Thomson, E. Ganz, J. Clarke, Phys. Rev. B 35 (1987) 7790.
[16] A. Selloni, P. Carnevali, E. Tosatti, C.D. Chen, Phys. Rev. B 34 (1986) 7406.
[17] N. Isshiki, K. Kobayashi, M. Tsukada, J. Vac. Sci. Technol. 9 (1991) 475.
[18] H.A. Mizes, S. Park, W.A. Harrison, Phys. Rev. B 36 (1987) 4491.
[19] N. Isshiki, K. Kobayashi, M. Tsukada, Surf. Sci. Lett. 238 (1990) L439.
[20] S. Hembacher, F.J. Giessibl, J. Mannhart, C.F. Quate, Proc. Natl. Acad. Sci. USA 100 (2003) 12539.
[21] J.S. Lukesh, L. Pauling, Am. Minerol. 35 (1950) 125.
[22] L. Pauling, Proc. Natl. Acad. Sci. USA 56 (1966) 1646.
[23] G. van Rossum, F.L. Drake, Python Reference Manual, PythonLabs, Virginia, USA, 2001, p. 1.
[24] R.A. Kendall, E. Apra, D.E. Bernholdt, E.J. Bylaska, M. Dupuis, G.I. Fann, R.J. Harrison, J.L. Ju, J.A. Nichols, J. Nieplocha, T.P. Straatsma, T.L. Windus, A.T. Wong, Comput. Phys. Commun. 128 (2000) 260.
[25] J.P. Perdew, K. Burke, M. Ernzerhof, Phys. Rev. Lett. 78 (1997) 1396.
[26] D.R. Hamann, Phys. Rev. B 40 (1989) 2980.
[27] E.J. Bylaska, P.R. Taylor, R. Kawai, J.H. Weare, J. Phys. Chem. 100 (1996) 6966.
[28] J.D. Bernal, Proc. Phys. Soc. A 106 (1924) 749.
[29] O. Hassel, H. Mark, Zeitschriftung fur Physik 18 (1924) 291.
[30] P. Trucano, R. Chen, Nature 258 (1975) 136.
[31] J. Tersoff, D.R. Hamann, Phys. Rev. Lett. 50 (1983) 1998.
[32] T.A. Land, T. Michely, R.J. Behm, J.C. Hemminger, G. Comsa, Surf. Sci. 264 (1992) 261.